

COBEM-2017-1465

CFD ANALYSIS ON HIGH-SPEED TRAIN AERODYNAMICS UNDER CROSSWIND CONDITIONS

Alexandre Felipe Medina

Federal University of Uberlandia, Av. Joao Naves de Avila, 2121, Uberlandia, Minas Gerais 38400-902, Brazil
alexandremedina@ufu.br, alexandremedina@icloud.com

Steve Cochard

Stadler Altenrhein AG, Industrie und Gewerbepark, 9423 Thal, Switzerland
steve.cochard@stadlerail.com

Francisco José de Souza

Federal University of Uberlandia, Av. Joao Naves de Avila, 2121, Uberlandia, Minas Gerais 38400-902, Brazil
francisco.souza@ufu.br

Abstract. Crosswind occurs as a train travels in windy conditions. The wind, combined with the train velocity, generates a relative wind that loads the train. This aerodynamic load can be strong enough to flip the train on its side. The purpose of this study is to assess the capabilities of RANS models on modeling the aerodynamics of high-speed trains under crosswind conditions. The CFD simulations are compared with respect to the DLR KKK wind-tunnel tests performed on the Stadler EC250 high-speed train. The validation of the numerical setup included the analysis of different turbulence models. The model that rendered best results was the SST transition model $\gamma - \text{Re}_\theta$. Good agreement was found between the wind-tunnel data and the simulation results, where the average deviation for the lee-rail moment coefficient is $\sim 6\%$, with maximum deviation of 9.8% at $\beta = 45^\circ$, which indicates a successful validation of the numerical data.

Keywords: Crosswind Stability, Train Aerodynamics, High-speed Trains, Computational Fluid Dynamics

1. INTRODUCTION

The first train accident caused by crosswind happened in St. Louis, United States of America, in April 1892, when a passenger train was blown from a narrow gauge track during a strong storm. In total, 29 crosswind-induced accidents have occurred since then, most of them in Japan due to the country's narrow gauge lines (Proppe & Wetzel, 2007; Peters, 2004). Recent crosswind-induced accidents includes two light trains in Europe (Austria, 2002 and Switzerland, 2007), a locomotive in Japan, 2006, and a 11-car train in China, 2007. Crosswind occurs as soon as a train travels in windy conditions. The wind, combined with the train velocity, generates a relative wind that loads the train. This aerodynamic load can be strong enough to flip the train on its side. The definition of a train traveling under crosswind condition is presented in Figure 1. The relative wind velocity V_a is the velocity between the train traveling speed V_{tr} and the wind velocity V_w . The yaw angle β is defined as the angle between the relative velocity and the train velocity and the wind angle φ between the train and wind velocities.

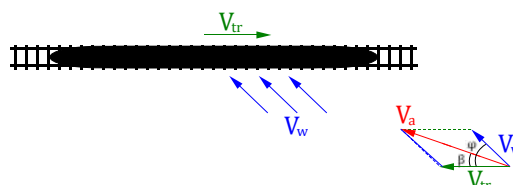


Figure 1. Definition of the crosswind condition for traveling trains.

To guaranty a safe operation on the European network all must follow the European Technical Specifications for Interoperability (TSI, 2008), which provide requirements to ensure the interoperability of the European rail systems. The TSI refers to the European Norms 14067 for aerodynamics (EN, 2010), which contains the trains certifications specifications. The procedures necessary for trains crosswind stability certification are presented in the EN-14067 "Part 6: Requirements and test procedures for crosswind assessment.

The EN-14067-6 standard requires that the aerodynamic analysis for the crosswind stability full proof for passenger trains with velocities between 200 and 360 km/h shall be done by static wind-tunnel tests. The norm requires static-models with low turbulence uniform inlet profile, ensuring reliability and repeatability. However, wind-tunnel testing does not fully represent the flow conditions observed at high-speed as the Reynolds number ($\sim 10^5$) is smaller compared to full-scale ($\sim 10^7$) and the static-models do not reproduce relative ground motion. Although wind-tunnel testing does not account for all the parameters encountered in the operation of a full scale train, the EN requirements assure the reproducibility of the results obtained for different facilities.

The purpose of this study is to evaluate the capabilities of the Reynolds-averaged Navier-Stokes (RANS) methodology for modeling the aerodynamics of high-speed trains under crosswind conditions with Computational Fluid Dynamics (CFD), in comparison to wind-tunnel measurements obtained for the Stadler EC250 high-speed train.

2. WIND TUNNEL MEASUREMENTS

Wind-tunnel tests provide the vehicle aerodynamic forces and moment coefficients, including the lee-rail moment coefficient $C_{M_{x,lee}}^*$, as it is mainly this moment that unload the windward wheels and could lead to vehicle overturning.. These coefficients are measured relative to a specific coordinate system according to the EN-14607 – 6. The origin of the coordinate system is located at the top-of-rail mid track position and half distance between the first-car bogies. The x direction points to the train direction of motion, y points to the lee-ward side of the train and z vertically towards the ground.

The full proof for crosswind stability for the Stadler EC250 was performed in the DLR Cryogenic Wind-tunnel Cologne (KKK) following the EN-14607 – 6. The KKK is a cryogenic closed-loop subsonic wind-tunnel with a test-section are of $32.34 m^2$. The high-speed train EC250 test model consists of a 1:25 scale 2-car static model, which results serve as our reference values. The tests were carried out on a Standard Single Track Ballast and Rail (STBR) ground simulation. Both model and STBR were installed on a splitter plate to avoid the wind-tunnel ground boundary layer influence, as presented in Figure 2a. The splitter plate is mounted on the wind-tunnel turn table and rotates with it. Once the wind-tunnel has reached the desired flow velocity, the turn table is rotated from 0° to 90° to simulate different yaw angles.

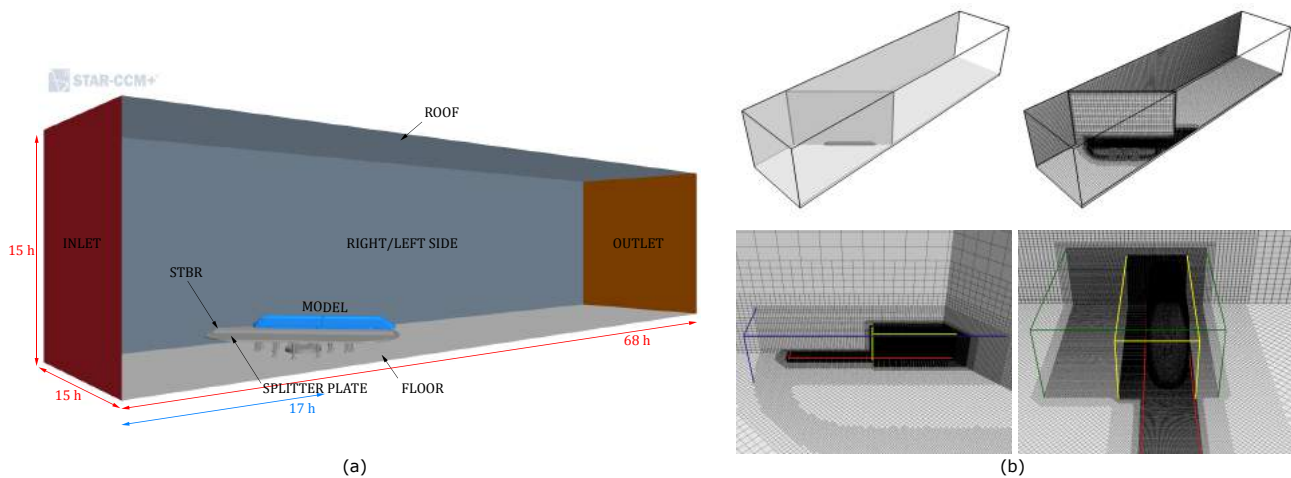


Figure 2. (a) Representation of the DLR KKK wind-tunnel test-section with the 2-car model, STBR configuration, splitter plate and stands. The dimensions are given with respect to the train height h . (b) Visualization of the mesh for CFD calculations.

3. VALIDATION

The results of the present calculations are obtained with the commercial solver STAR-CCM+ version 11.02 from CD-adapco, which solves the Navier-Stokes equations using a finite-volume method. In this study the flow is considered steady and the Navier-Stokes equations are simplified by time-averaging, resulting in the Reynolds-Averaged Navier-Stokes equations (RANS). Different RANS turbulence models were analyzed in the validation phase to determine the one that gives the best results. These turbulence models are the $\kappa - \varepsilon$ class v^2f model (Davis et al. , 2012) and Elliptic Blending model (Billard et al. , 2011), the $\kappa - \omega$ class standard shear stress transport (SST) model (Menter , 1993) and SST γRe_θ model (Menter et al., 2004), and the Reynolds Stress Transport (RSM) model (Launder et al., 1975).

A detailed reproduction of the DLR KKK wind-tunnel was produced to validate the CFD simulations. The 1:25 EC250 2-car model, STBR and splitter plate with stands were modeled to ensure complete similitude between experimental and simulated flow, as seen in Figure 2a. The boundary conditions used in the calculations are as follows:

1. block profile velocity-inlet condition corresponding to $Re = 7.0 \cdot 10^5$ based on train height;
2. no-slip wall boundary condition applied to the sides, floor and roof of the wind-tunnel test section and the train surfaces;
3. pressure-outlet boundary condition with $0 Pa$ applied at surface.

The computational mesh consist of a trimmed mesh with prism layers applied at the model surfaces, shown in Figure 2b. The prism layer mesh was refined to achieve the required dimensionless wall-distance y^+ for each turbulence model. Models as the SST class and RSM resolve the viscous sublayer directly, but requiring a fine prism layer mesh with a $y^+ < 3$. Models as the $\kappa - \varepsilon$ class use a coarser prism layer mesh by using wall functions, hence a $y^+ > 30$ can be applied. To fulfill this requirements, 12 prism layers were applied for the SST and RSM models and 6 prism layers for the $k - \varepsilon$ models, with a prism layer growth ratio of 1.5. The mesh resolution plays an important role in the accuracy of the results and it is important to refine it in regions of strong gradients. Four refinement levels were applied to resolve the flow in the leeward side wake and the under-body region. The described mesh settings applied to the computational domain is referred in this study as Case A. The mesh setup was maintained for all the analysis of the present study with refinement levels applied at regions of strong gradients as the train lee-side and under-body regions. Modeling the full KKK would require not only a fine mesh in the wake and under-body regions of the flow, but also in the region between the stands, under the splitter plate. Modeling the flow under the splitter plate requires a large number of cells, increasing the CPU time to reach a solution.

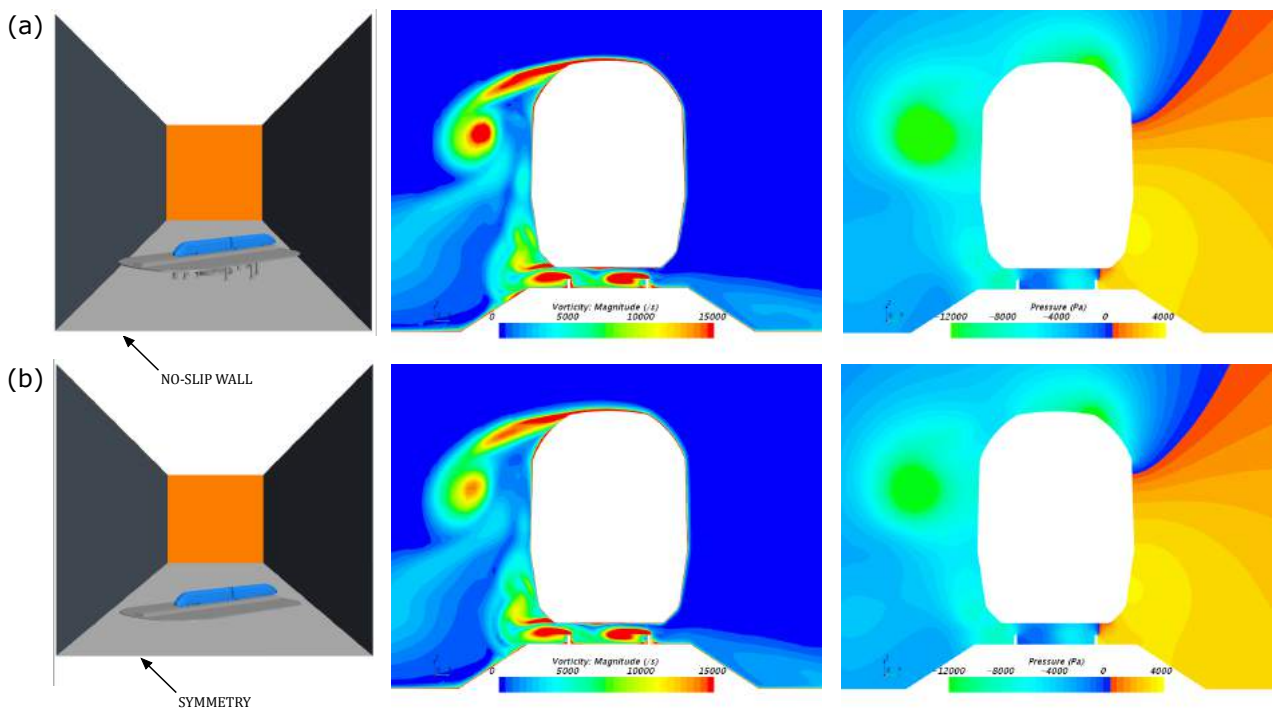


Figure 3. Analysis of the vorticity and pressure fields for the full DLR KKK wind-tunnel, Case A (a) and symmetry plane, Case B (b). Results obtained with the standard SST turbulence model for yaw angle $\beta = 45^\circ$. *Plane I*, located $200 mm$ ahead of the measuring coordinate system, or $356 mm$ aft the nose of the leading-car.

To avoid spending resources on the flow under the splitter plate, a symmetry plane condition was applied in its horizontal half. This symmetry plane reduces by 20% the number of cells, resulting in a mesh with approximately $160 \cdot 10^6$ cells, keeping the aerodynamic coefficients within 1%. This 20% reduction in cells number led to a CPU time 15% lower. This computational domain is referred as Case B. Similar results are achieved between Case A and B, as shown in Figure 3. As the aerodynamic coefficients and flow topology are similar, the setup with the symmetry plane, Case B, was chosen to carry on the simulations.

A mesh dependency test was performed with the SST $\gamma - Re_\theta$ turbulence model using a coarse and a medium resolution mesh ($130 \cdot 10^6$ and $140 \cdot 10^6$ cells, respectively) compared to our fine mesh setup applied to Case B ($160 \cdot 10^6$ cells). The results are within $\pm 2\%$ of the present finer mesh, as presented in Figure 4 for yaw angle $\beta = 45^\circ$. Thus the results can be considered mesh independent.

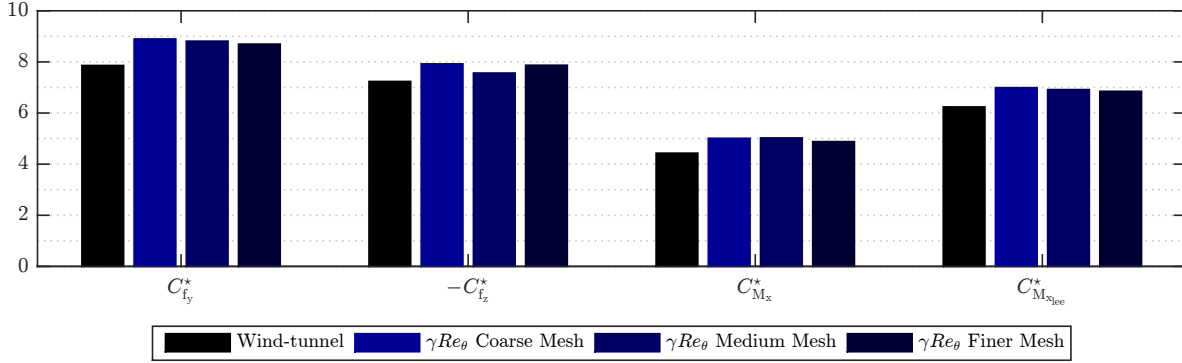


Figure 4. Mesh dependency analysis of the side force, lift, rolling moment and lee-rail moment coefficients, Case B with SST $\gamma - Re_\theta$ model at $\beta = 45^\circ$.

The results obtained from the different turbulence models analyzed are presented in Figure 5 for yaw angle $\beta = 45^\circ$. The overall behavior of the aerodynamic coefficients, with larger differences found for the force coefficient $C_{f_z}^*$. It is observed that an increase of the side force is followed by a decrease of the lift force coefficient, and vice-versa, resulting in a close rolling and lee-rail moment coefficients for all the models, as also reported by Diedrichs (2008).

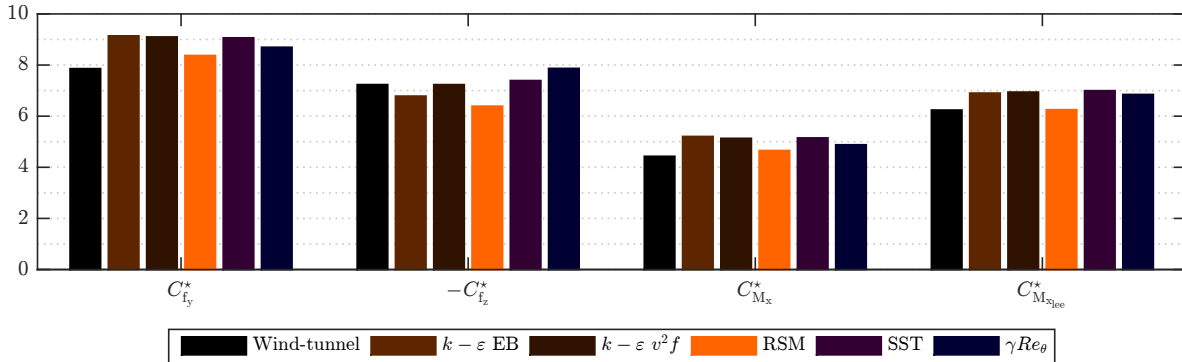


Figure 5. Turbulence model analysis of the side force, lift, rolling moment and lee-rail moment coefficients. Case B at $\beta = 45^\circ$.

Both the RSM and SST $\gamma - Re_\theta$ models displayed better overall performance compared to the other turbulence models, mainly for $C_{f_y}^*$, $C_{M_x}^*$ and $C_{M_{x_{lee}}}^*$. However, the RSM model underestimates the lift coefficient by a larger extent than the other models. Although the SST $\gamma - Re_\theta$ model overestimates the aerodynamic coefficients, its average deviation is less than other $\kappa - \epsilon$ class and standard SST models.

Performing a cost-effective analysis for both RSM and SST $\gamma - Re_\theta$ turbulence models, the RSM requires larger CPU time, as it is a seven-equation model. As the four-equation SST $\gamma - Re_\theta$ model produces reliable results in less CPU time it was chosen to carry on the parametric studies presented in the analysis section, present in the full paper.

The validation of simulations from $\beta = 05^\circ$ to 50° was carried out with the SST $\gamma - Re_\theta$ turbulence model and the presented mesh setup, with $160 \cdot 10^6$ cells. The comparison between the simulation results is presented in Figure 6. The average deviation for the lee-rail moment coefficient is $\sim 6\%$, with maximum deviation of 9.8% at $\beta = 45^\circ$, which indicates a successful validation of the numerical data.

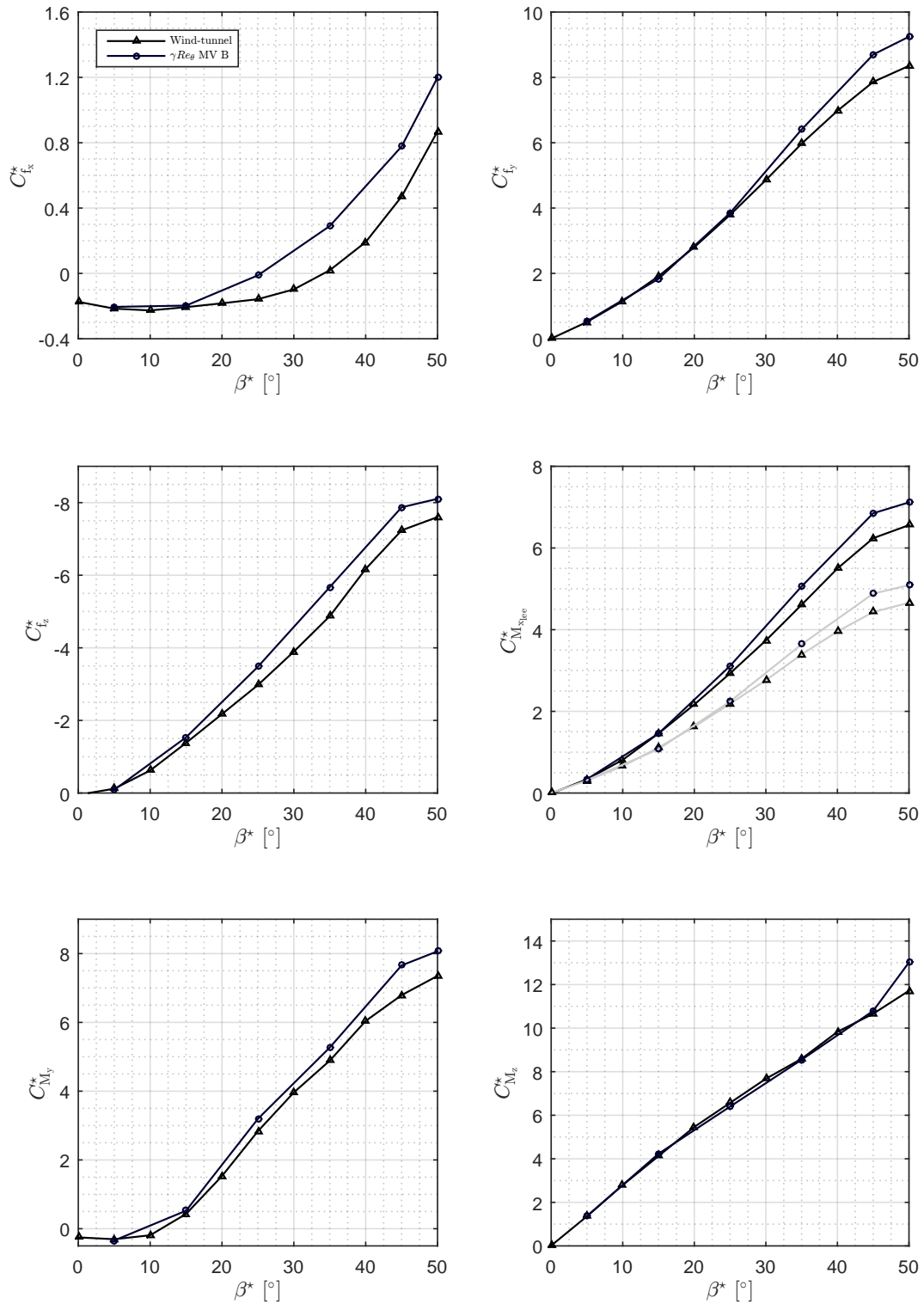


Figure 6. Validation results for the aerodynamic coefficients from $\beta = 0^\circ$ to $\beta = 50^\circ$, from Case B for the SST $\gamma - Re_\theta$ turbulence model (the results for the rolling moment coefficient $C_{M_x}^*$ are presented in light gray).

The comparison between the simulation results with the SST $\gamma - Re_\theta$ model and the KKK wind tunnel results, obtained with Particle Image Velocimetry (PIV), is given in Figure 8 and Figure 7, comparing the vector field colored with the $\lambda - 2$ criterion for both cases. There is fair agreement between the simulation and wind tunnel analysis, as the position of the wake vortex is similar for both cases. At lower yaw angles (Figure 8) both the vortex position and strength are in agreement between the simulation and the wind tunnel experiments. This is in accordance with what is found for the aerodynamic coefficients for these yaw angles (see Figure 6). However, at higher yaw angles we can see that the simulation renders a stronger vortex (Figure 7), leading to the over-prediction of the aerodynamic coefficients.

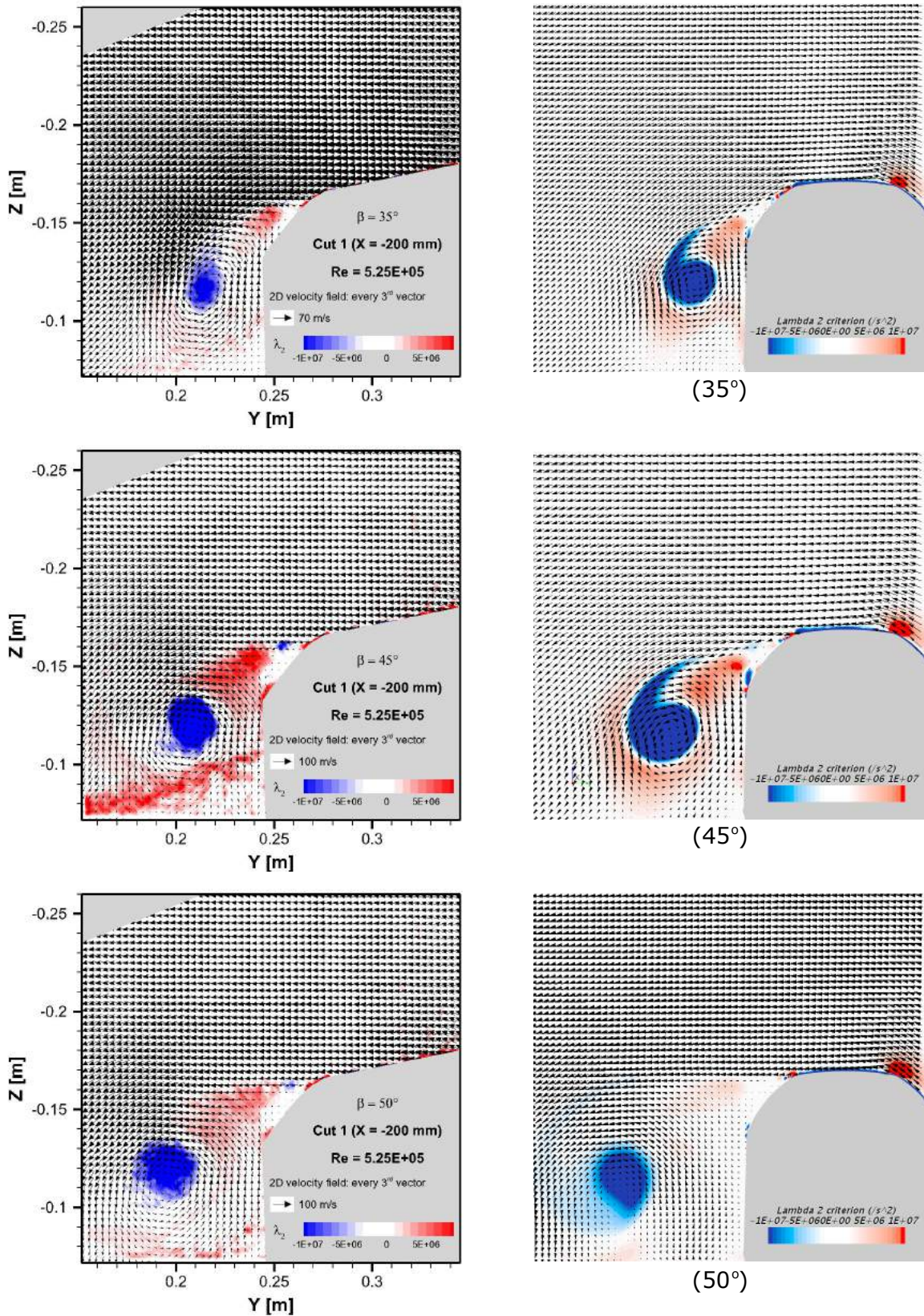


Figure 7. Comparison between the simulation results from Mesh V, Domain B, SST $\gamma - Re_\theta$ turbulence model, with respect to the KKK wind tunnel results for yaw angles $\beta = 35^\circ$, $\beta = 45^\circ$ and $\beta = 50^\circ$. Vector field colored with the $\lambda - 2$ criterion at *Plane I*, located 200 mm ahead of the measuring coordinate system, or 356 mm aft the nose of the leading-car.

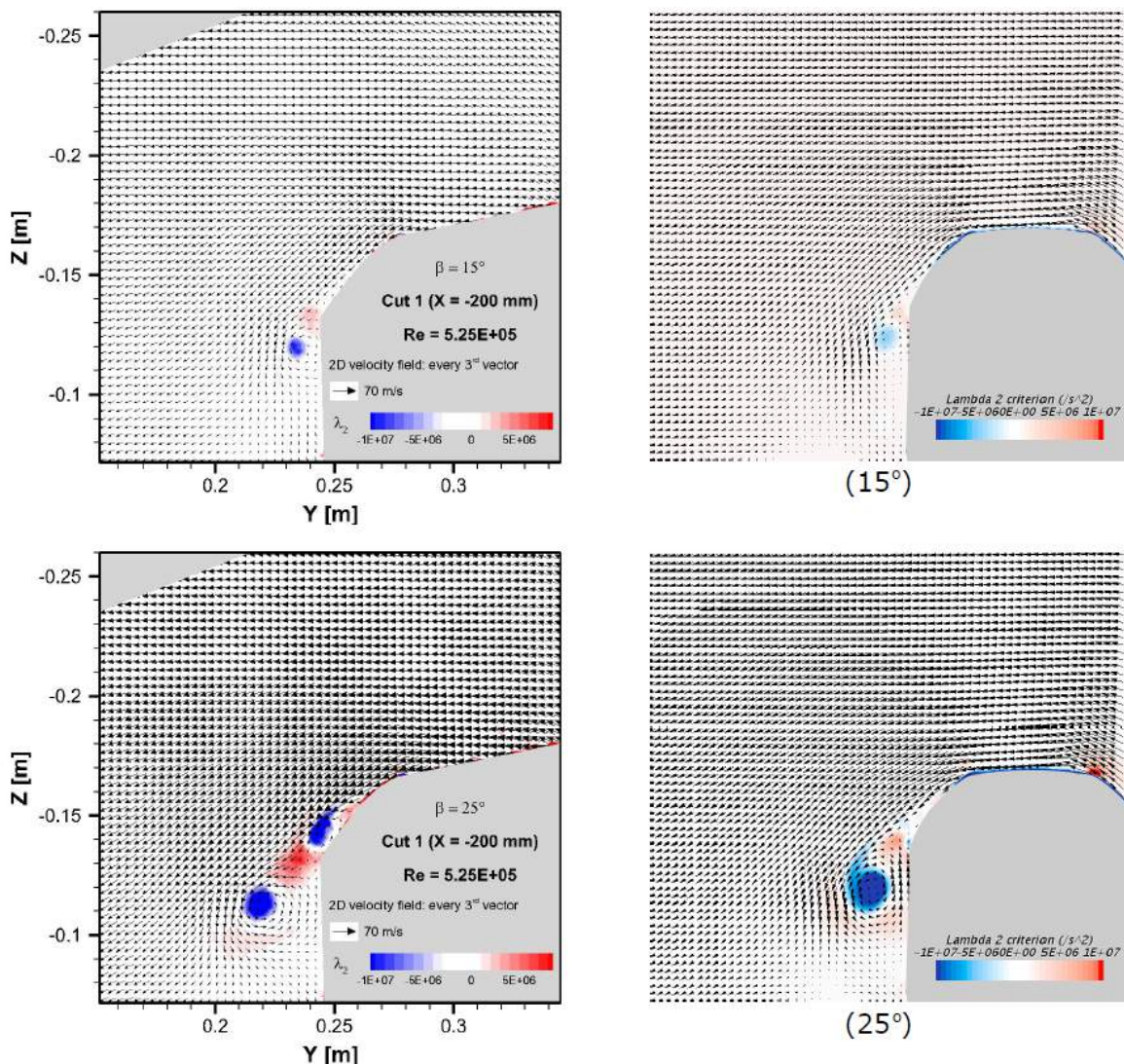


Figure 8. Comparison between the simulation results from Mesh V, Domain B, SST $\gamma - Re_{\theta}$ turbulence model, with respect to the KKK wind tunnel results for yaw angles $\beta = 15^{\circ}$ and $\beta = 25^{\circ}$. Vector field colored with the $\lambda - 2$ criterion. Evaluation made for *Plane I*, located 200 mm ahead of the measuring coordinate system, or 356 mm aft the nose of the leading-car.

4. CONCLUSION

Computational Fluid Dynamics (CFD) was used to study the influence of the wind-tunnel setup on the aerodynamic coefficients. Even if transient Delayed Detached Eddy Simulations (DDES) showed better potential than steady-state ones for yaw angle above 30° , this study restricted itself to RANS simulations for time and resources reasons. From all the tested RANS turbulence models, the Reynold Stress Model (RSM) and the Shear Stress Transport (SST) with the $\gamma - Re_{\theta}$ transition model gave the overall best results on our finer mesh (Mesh V). The SST $\gamma - Re_{\theta}$ was chosen over the RSM for two reasons: 1) it does not under-estimate C_{f_z} and 2) it converged quicker.

Good agreement between the simulation results and the wind-tunnel data was found for yaw angles ranging from 5° to 50° , shown in Figure 6. Fair agreement was also found for the $\lambda - 2$ criterion colored vector fields for different yaw angles, for both wake intensity and position. Thus, we conclude that our CFD setup is validated and it is possible to proceed to analyze the influence of the moving model and, in sequence, whether the train stability is affected by its air intake and exhaust systems. The good agreement of our results shows the capabilities of RANS models applied to industrial flows.

5. ACKNOWLEDGEMENTS

The authors would like to thank Stadler Altenrhein AG for the financial and computational support, CD-adapco for providing the academic license, and the development agencies FAPEMIG, CNPq and CAPES, from the Brazilian government.

6. REFERENCES

- Proppe, C.; Wetzel, C. Overturning Probability of Railway Vehicle under Wind Gust Loads. In: *Proceedings of the IUTAM Symposium on Dynamics and Control of Nonlinear Systems with Uncertainty*. Nanjing: Springer, 2007. p.23–32. ISBN 9781402063312. ISSN 18753507.
- Peters, J. L. How to Reduce the Cross Wind Sensitivity of Trains. In: *The Aerodynamics of Heavy Vehicles: Trucks, Buses, and Trains*. 19. ed. Berlin, Heidelberg: Springer Berlin Heidelberg, 2004. cap. 40, p. 453–467. ISBN 978-3-540-44419-0.
- TSI-HS-RST. Technical specification for Interoperability relating to the Rolling Stock sub-system of the trans-European high-speed rail system. (2008/232/CE), 2008.
- EN-14607-6. Requirements and test procedures for cross wind assessment. European Standards, 2010.
- Davis, P. L.; Rinehimer, A. T.; Uddin, M. A comparison of RANS-based turbulence modeling for flow over a wall-mounted square cylinder. In: *20th Annual Conference of the CFD Society of Canada*. Canmore: [s.n.], 2012. p. 8.
- Billard, F.; Laurence, D. A robust k-epsilon $v2/f$ elliptic blending turbulence model with improved predictions in near-wall, separated and buoyant flows. *International Journal of Heat and Fluid Flow*, v. 44, p. 1–25, 2011.
- Menter, F. R. Zonal Two Equation Kappa-Omega Turbulence Models for Aerodynamic Flows. In: *24th AIAA Fluid Dynamics Conference*. Orlando, FL: AIAA, 1993. p. 22.
- Menter, F. R. et al. A Correlation-based Transition Model Using Local Variables: Part I Model Formulation. In: *Proceedings of the ASME Turbo Expo, Power for Land Sea and Air*. Vienna: ASME, 2004. p. 57–67. ISBN 0-7918-4169-3.
- Launder, B.; Reece, G. J.; Rodi, W. Progress in the development of a Reynolds-Stress turbulent closure. *Journal of Fluid Mechanics*, v. 68, n. 3, p. 537–566, 1975. ISSN 0022-1120.
- Diedrichs, B. Aerodynamic calculations of crosswind stability of a high-speed train using control volumes of arbitrary polyhedral shape. In: *BBA VI International Colloquium on: Bluff Bodies Aerodynamics & Applications*. Milano: [s.n.], 2008. p. 20–24.

7. RESPONSIBILITY NOTICE

The authors are the only responsible for the printed material included in this paper.